ISSN 2816-573X

ORIGINAL ARTICLE

Computation Investigation on Doped Graphene for Advanced Electronic Structure: A First-Principles Investigation with Indium and Antimony

Riddhisiddhiba Zala[1], Drashti Sagpariya[1], Gaurav Jadav[2], Sandhya Dodia[3], Tanvi Dudharejiya[1], Nirali Udani[1], DK Dhruv[4], VD Bhatt[2], JH Markna[1], Bharat Kataria[1*]

Zala R, Sagpariya D, Jadav G, et al. Computation Investigation on Doped Graphene for Advanced Electronic Structure: A First-Principles Investigation with Indium and Antimony. Int J Adv Nano Comput Anal. 2024;3(2):43-55.

Abstract

This study investigates the impact of Indium (In) and Antimony (Sb) doping on the electronic properties of graphene using Density Functional Theory (DFT) for structure optimization calculations. The doping effect was analyzed with dopant concentrations of 0.72% (two dopant atoms) and 2.88% (eight dopant atoms). The results show that doping graphene with In and Sb produces p-type and n-type semiconductors, respectively. As the quantity of dopants increases, graphene transitions from a semimetal to a semiconductor. Specifically, the band gaps for graphene doped with two and eight atoms of In are 0.5451 eV and 0.1443 eV, while those doped with two and eight atoms of Sb are 1.5684 eV and 0.5726 eV, respectively. These findings provide a pathway for tailoring the electronic properties of graphene, offering potential applications in nanoelectronics, optoelectronics, and energy storage devices.

Key Words: *Graphene; Electronic properties; Doping; Indium; Antimony; Band engineering; Density of States (DOS)*

Introduction

The development of computational methods to solve the Schrodinger wave equation has undergone significant milestones, with early contributions from D.R. Hartree, J.C. Slater, and others. In 1928, Hartree introduced a method for calculating the characteristic values of the Schrödinger equation in a non-Coulombic central field, where the potential varies with the distance rrr from the nucleus. He modified the equation to ensure a finite solution at r=0r = 0r=0 and approached zero at r=∞. Hartree's approach was crucial for approximating energy parameters and solving the Self-Consistent Field

[1]*Department of Nano Science and Advanced Materials, Saurashtra University, Rajkot-360005, Gujarat, India*
[2]*School of Applied Science and Technology, Gujarat Technological University, Ahmedabad- 382424, Gujarat, India.*
[3]*Gujarat Technological University, Ahmedabad- 382424, Gujarat, India*
[4]*Natubhai V. Patel College of Pure and Applied Sciences, Vallabh Vidyanagar, 388120 India*

[*]*Corresponding author: Bharat Kataria, Professor, Department of Nano Science and Advanced Materials, Saurashtra University, Rajkot-360005, Gujarat, India, Email: brkataria22@rediffmail.com*
Received: November 18, 2024, Accepted: November 25, 2024, Published: December 06, 2024

(SCF) equations for various atomic systems like He, Na+, and Cl-, with results showing strong agreement with experimental X-ray parameters and charge distributions [1,2].

Building on Hartree's work, J.C. Slater (1928) reviewed and improved upon his method. Slater introduced perturbation theory to refine energy levels, highlighting the need for more accurate treatments of electron distribution, resonance interactions, and polarization effects [3]. Fock (1930) expanded on these ideas, developing self-consistent field equations that included exchange terms, resulting in more precise solutions for electron systems and laying the foundation for modern computational quantum mechanics [4,5]. In 1927, L.H. Thomas further contributed by introducing a method to calculate atomic constants from the effective electric field within an atom, especially for heavy elements, facilitating more accurate theoretical computations [6]. The advent of Density Functional Theory (DFT) marked a new era in computational chemistry. Hohenberg and Kohn's groundbreaking work in 1964 established the foundation for DFT by introducing a universal density functional that could describe the ground-state energy of an electron system in an external potential, regardless of the specific form of the potential. This work was later expanded by Kohn and Sham (1965), who introduced the self-consistent equations that incorporate exchange and correlation effects, which are essential for accurate simulations of electron behavior in complex systems [7,8].

In realm of graphene doping, diverse materials, and elements have been explored to tailor electronic properties for specific applications. First and foremost, graphene doped with Boron (B), Nitrogen (N), Oxygen (O), and Fluorine (F) at a 2% concentration revealed intriguing semiconductor behavior [9-15]. B-doped graphene experienced a blue shift towards larger energies, with diminishing peak intensities correlating with the influx of electrons into the structure, showcasing the tenability of graphene's electronic structure. In the realm of composite materials, the incorporation of Germanium Sulfide (GeS) into graphene-based Field-Effect Transistor (FET) devices demonstrated noteworthy outcomes. The presence of GeS resulted in the formation of a p-type layer, which signifies an excess of positive charge carriers and an increase in conductivity. Furthermore, the resulting connection demonstrated a substantial enhancement in structural stiffness and anisotropy, highlighting the potential of GeS/graphene composites for sophisticated electronic applications. Expanding beyond the practice of introducing small amounts of impurities, the investigation encompassed the use of Aluminium (Al) and Nitrogen (N) to introduce impurities into graphene sheets. The concentrations of these impurities ranged from 2% to 12%. This experiment revealed a progressive transformation of graphene, shifting from a semi metallic state to a semiconducting one as the number of dopants increased. Al-doping induced p-type semiconductor behavior, while N-doping resulted in n-type characteristics. These findings highlight the versatility of graphene in adopting distinct electronic properties based on the nature and concentration of dopants. Table 1 shows the study of different doping material effects on Carbon allotrope such as Graphene, GeS/Graphene, poly (9-vinyl carbazole)/graphene, $C_{31}XH_{14}$, and $C_{53}XH_{18}$ (X = N, Pt, Fe, B, Al, Ni, and P).

TABLE 1
Effect of different doping on carbon allotrope.

Sr. No.	Materials	Doped Atoms	Doping Concentration	Impacts	Reference
1.	Graphene	B, N, O, and F	2%	Boron-doped graphene exhibits p-type semiconductor behavior, whereas configurations containing nitrogen (N), oxygen (O), and fluorine (F) have n-type characteristics based on their respective band gaps. The absorption peaks have undergone a blue shift, meaning they have changed towards higher energies. Additionally, the peak intensities decrease as additional electrons enter the structure.	[9]
2.	GeS/Graphene			Germanium sulphide (GeS) functions as a p-type layer in field-effect transistor (FET) devices based on graphene. Moreover, the connection exhibits significantly enhanced structural rigidity and anisotropy.	[10]
3.	Graphene	Al and N	2% to 12%	Doping with Al and N led to the creation of p-type and n-type semiconductors within the graphene sheet. As the number of dopants grows, graphene undergoes a shift from being a semimetal to becoming a semiconductor.	[11]
4.	$C_{31}XH_{14}$ and $C_{53}XH_{18}$	X = N, Pt, Fe, B, Al, Ni, and P	2% to 10%	The DOS plots of the graphene models reveal that intrinsic and Pt graphene possess non-magnetic properties, while Fe and Ni-doped graphene exhibit magnetic characteristics. The energy levels of P-type dopants (B and Al) show a change towards higher energy levels in their DOS peaks, while the energy levels of n-type dopants (N and P) show a shift towards lower energy levels in their DOS peaks.	[12]
5.	Graphene	B and N	2% to 12%	As the quantity of dopants increases, the electronic characteristics change from semimetal to semiconductor. Band gap changes when alternative doping locations are considered for the same substitutional doping concentration. The band gap reaches its maximum value when dopants are located at identical sub-lattice positions, and it decreases when dopants are put at alternating sub-lattice positions.	[13]
6.	Graphene	B, N, and BN	2% to12% for B, N and 4% to 24% for BN	Doping with boron (B) and nitrogen (N) individually results in the creation of a band gap at the Dirac point, which in turn causes a displacement of the Fermi level. Introducing BN through co-doping induces a band gap at the Fermi level, leading to enhanced efficiency.	[14]
7.	poly(9-vinyl carbazole)/ graphene(PVK/ GR)			The PVK/GR Nano heterostructure composite, characterized by a narrow band gap and exceptional stability, shows promising potential for use in solar systems.	[15]

This study conducted a first-principles inquiry to analyze the band structure properties and DOS of graphene sheets that were uniformly doped with antimony and indium atoms, among other elements. Indium and antimony were selected as dopants due to their unique ability to induce distinct p-type and n-type semiconductor behaviors in graphene. Indium, with one fewer valence electron than carbon, acts as a p-type dopant, shifting the Fermi level below the Dirac point and enhancing hole carrier concentration. Conversely, antimony, with one additional valence electron, serves as an n-type dopant, elevating the Fermi level above the Dirac point and increasing electron carrier concentration. This dual nature enables a broad spectrum of electronic modifications, making In and Sb ideal candidates for tailoring graphene's band structure. Their effectiveness in altering graphene's semimetallic properties into semiconducting behavior demonstrates their potential for applications in advanced electronic and optoelectronic devices. There is no gap in doped graphene at the Dirac point, but this relies on how dense the dopant atoms are. The electrical structure and DOS computations were conducted using the Burai software code, an advanced Graphical User Interface (GUI) system specifically developed for the Quantum Espresso code. The exchange-correlation energy of electrons was calculated using the Generalized Gradient Approximation (GGA) within the framework of first principal DFT.

Computational technique

The theoretical framework of our study is grounded in first-principles calculations, a powerful approach based on quantum mechanics. DFT serves as the cornerstone of our computational methodology, providing a reliable and accurate foundation for simulating the electronic structure of materials [16]. The chosen DFT method allows us to consider the quantum mechanical interactions between electrons and nuclei, providing a comprehensive understanding of the system under investigation. Our simulations involve the creation of graphene supercells, where indium and antimony atoms are strategically placed within the graphene lattice. Subsequently, the analysis focuses on the interactions between these dopants and the carbon atoms, considering variables such as the lengths and angles of the bonds, as well as the electronic states. We figured out the electronic band structures of the doped graphene systems, which show how adding indium and antimony changes the energy levels and conductivity of the material.

Quantum espresso based DFT calculations (which are frequently used for computationally modeling the quantum mechanics that are used to investigate the electrical the arrangement and organization of complex systems such as atoms, molecules, and condensed phases) have been utilized for the theoretical analysis to gain insight into the electrical and optical characteristics of Graphene. The present work utilizes the Graphical User Interface (GUI) of Quantum Espresso BURAI 1.3 to perform first-principles calculations based on Density Functional Theory (DFT). BURAI simplifies the setup and visualization of complex systems, allowing for seamless execution of DFT simulations. It aids in configuring the input parameters, setting up supercells, and conducting electronic structure calculations, ensuring an efficient and user-friendly approach to modeling the properties of doped graphene. Specifically, the study focused on calculating the electrical and band gap structural features of pure graphene and graphene doped with Indium (In) and Antimony (Sb). Burai constructed a hexagonal structure from the CIF (Crystallographic Information File) file downloaded from materials square [17]. Adding to the information, the CIF format is a standard file format used for representing crystallographic information. It includes information about the atomic positions, the size of the unit cell, the symmetry operations, and other factors that are required to characterize the crystal structure of a material. We utilize the first principle calculation DFT for improved

electronic properties and better determination of energy band gap values [18].

Methodological approach and computational details

The QUANTUM ESPRESSO code version 1.3 is utilized for all calculations, employing the DFT method. A vacuum layer of 15Å was introduced along the z-axis to prevent interactions between periodic images in the supercell. This sufficiently isolates the graphene sheet from its periodic copies. For k-point sampling, a 2x2x2 Monkhorst-Pack grid was used to sample the Brillouin zone. This grid provides a good balance between computational efficiency and accuracy, ensuring proper sampling of the electronic structure without introducing significant computational overhead. The GGA refers to the "Perdew-Burke-Ernzerhof" parameterization [19,20]. We utilized ultra-soft pseudopotentials to accurately represent the interactions between electrons and ions. The plane wave basis sets method was employed to characterize the exchange-correlation function [21].

The plane-wave energy cutoff was set at 25 Ry for the wavefunction and 225 Ry for the charge density. These values were determined based on convergence tests that ensure accurate results without excessive computational cost. The chosen cutoffs are sufficient for the systems studied, as they provide convergence within a few millielectronvolts (meV) for total energy calculations, which is critical for the precision of electronic structure and bandgap predictions in graphene-based systems. -48.71Ry was the energy convergence value. Since the element is Semi-metal, Fermi-Dirac with smearing electron occupation. The smearing width is 1.00000e-02 Ry. The k-point of the Brillion zone sampling mesh parameter is 2×2×2. A 3×3 supercell, containing 36 carbon atoms, was employed to model the isolated sheet. To prevent inter-layer interactions, all sheets were separated by more than 15Å in the perpendicular directions, as depicted in Figure 1. The doping concentration was determined by approximating the ratio of doped atoms to the total number of atoms in graphene. Specifically, it was calculated by dividing the number of doped atoms by the total number of atoms within a 36-carbon unit cell, which was confirmed using appropriate software tools.

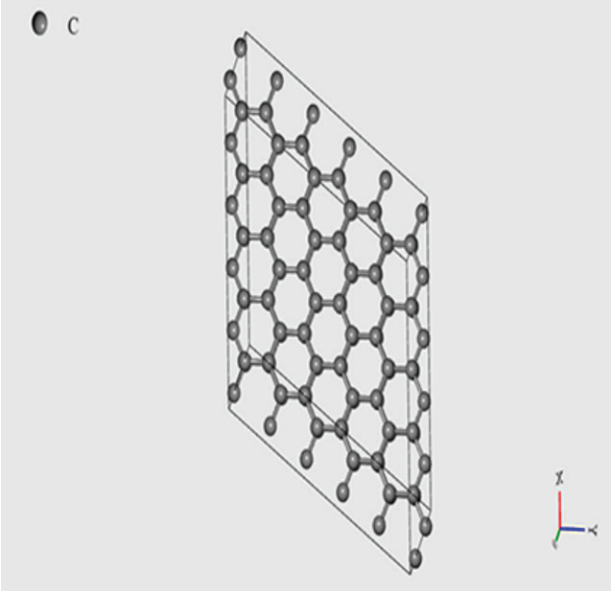

Figure 1) *Crystal structure of graphene.*

The Monk-Horst pack scheme is employed for sampling the Brillion zone. The band structure was computed along high-symmetry points in the Brillouin zone (Γ, K, and M points). These points were selected because they represent key features of the electronic structure in graphene's hexagonal lattice, particularly around the Dirac point. The choice of these path points allows for a detailed analysis of the electronic bandgap and the overall dispersion behavior of the material. The Fermi-Dirac smearing technique was employed to compute the partial occupancies of each wave function. The lattice parameters of this supercell are a=b=2.47Å and c=7.80Å, with α=β=90°, γ=120°, and a C-C bond length of 1.42Å. The lattice parameter has a volume of 41.14Å. Table 2 displays the input parameters, specifically the places on the walk path, that are used for band structure computations. These are the structural characteristics of graphene in its pure form as determined by crystallography [15].

TABLE 2
Input parameter (points on walk path) for band structure calculation.

Point on walk path	nk
gG	20
M	20
K	20
gG	20
A	20
L	20
H	20
A	0
L	20
M	0
K	20
H	0

Results and Discussions

Electronic properties refer to the properties of a material that are related to its electronic structure and behavior. Here, we are going to discuss the two main electronic properties which are Band Gap & DOS. The electronic properties of a substance can be found by analyzing the distribution of energy levels within the electron's valence and conduction bands. An accurate description of these electronic properties requires an understanding of how the individual orbitals contribute to the overall electronic structure of the material. To successfully complete a band structure computation, one must calculate an integral throughout the crystal Brillion zone. Quantum Espresso performs numerical integration in a preliminary stage, so the primary criteria are the choice of plotting points. The Brillion zone in graphene consists of a two-dimensional hexagon. An ideal material is semi-metallic, exhibiting alignment between the Fermi level and the Dirac point, and the absence of unbound electrons in the conduction band at absolute zero temperature.

Pure graphene

Computational quantum chemistry, SCF stands for Self-Consistent Field. It is an iterative strategy for solving problems with the molecular and material's electrical configuration. The SCF approach necessitates an initial approximation of the electrical wave function, which is then utilized to compute the electron density and electronic energy. The computed energy is then compared to the previous iteration, and if it has not converged (achieved a stable value), the wave function is changed based on the current density. This process is repeated until the electronic energy achieves the necessary level of accuracy. Convergence is important in the SCF calculation because it ensures that the electronic structure is accurately represented. When the SCF process converges, it means that the electronic wave function and density have reached a stable state, and the computed energy provides a reliable estimate of the actual electronic energy of the system. Achieving convergence guarantees that the derived properties and observables, such as band energies, bond length and spectroscopic properties, are reliable, otherwise, the calculated

properties may be unreliable. SCF of pure graphene converges with -48.71462470 Ry energy.

The DOS curves typically show two main regions: one is the valence band, and another one is the conduction band. The valence band encompasses the energy levels where electrons are present in their lowest energy state, The conduction band encompasses the energy levels that electrons can reach when they are stimulated to higher energy states. The DOS in the valence band is relatively high and extends over a broad energy range, while the DOS in the conduction band is lower and more sharply peaked. As shown in Figure 2 in this band gap, there is peak at fermi energy value. In Figure 3, the graph depicting the relationship between Integrated Density of State (IDOS) and E generally displays a staircase-like structure, whereby each step represents the proportion of electronic states that fall within a certain energy range. The Fermi level, often represented as EF, serves as a fundamental reference point that signifies the electronic state with the maximum capacity at absolute zero temperature. The examination of the variation in the IDOS concerning the Fermi level provides valuable insights on the conductive characteristics of the material and its capacity to accept charge carriers. The Integrated DOS vs Energy graph at a 5.426 eV Fermi level has a unique pattern, suggesting a special arrangement of electronic states inside the material. The presence of peaks and troughs in the staircase-like pattern provides valuable information on the conductive property and band structure of the material, which is essential for comprehending its electrical characteristics.

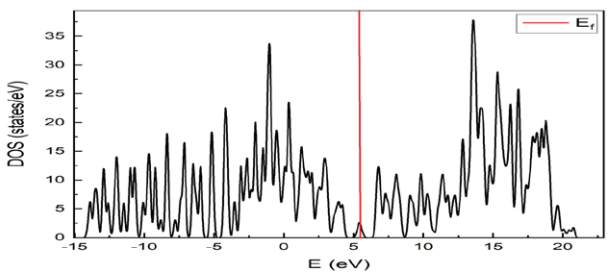

Figure 2) *DOS in the pristine crystal structure of graphene.*

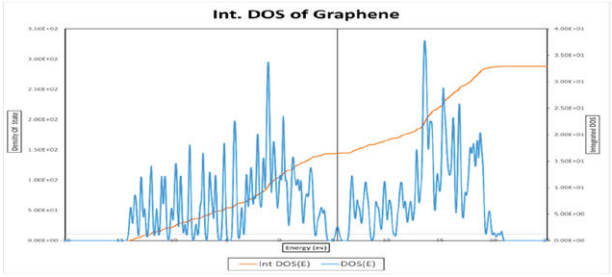

Figure 3) *Integrated DOS of pure graphene crystal structure.*

The electric band structure for a pure graphene structure is illustrated in Figure 4. In general, VBM and CBM values influence the material's band gap energy. The energy dispense of electrons within the valence band and conduction bands can be Used to forecast the properties of solid electronic materials. The grey region indicates the basic gap. As shown in the image, the conduction and valence bands intersect at the Fermi level, resulting in a band gap of zero. Graphene exhibits a pleasing linear dispersion relation at the Dirac point.

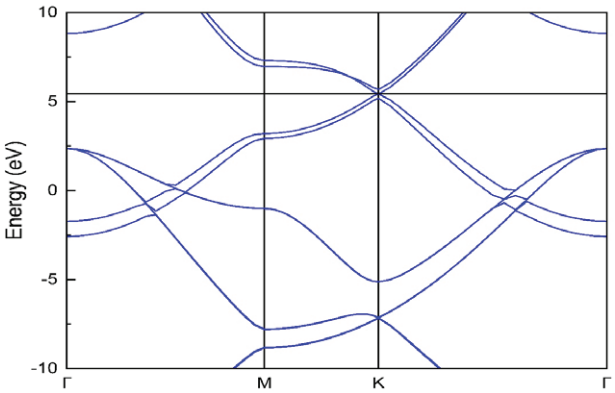

Figure 4) *Pure graphene band structure.*

Indium-doped graphene

The pure graphene is doped with In atoms at concentrations of 0.72% (In_2C_{34}) and 2.88% (In_8C_{28}) as shows in Figure 5, depicts the doping of In atoms in graphene. The electronic properties, specifically the band structure and DOS, it might be approximated using the previously mentioned computational technique. In the presence of an In-dopant, the Fermi level is lowered towards its valence band, The reason for this is that the In atom has one fewer electron than a C atom, which allows it to function as a p-type dopant. This result is consistent with

before theoretical and experimental studies. Fermi levels shift dramatically below the Dirac point, resulting in p-type doping. This modifies the behaviour of graphene. When a solitary indium atom is introduced into a graphene sheet, it undergoes sp_2 hybridization.

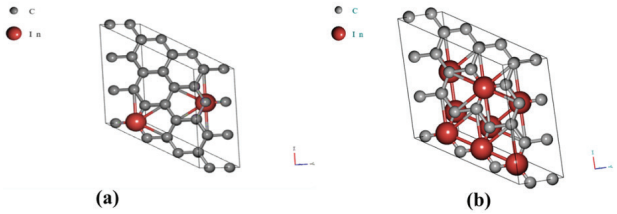

Figure 5) *Crystal structure of indium doped graphene for DFT.*

In_2C_{34} (0.72%)

Now we have modified the calculated values of SCF for 0.72% In doping cells. As a result, the obtained values are steady and do not change. Convergence has been achieved in 11 iterations with a -697.48081263 Ry energy.

The In-doped graphene In_2C_{34} crystal structure's entire DOS is depicted in Figure 6. The peak reveals that the Fermi level of graphene doped with indium descends beneath the Dirac point, signifying its classification as a p-type semiconductor [22]. Figure 7 shows the IDOS which give a Fermi energy value. In_2C_{34} has an EF of 6.706 eV. Doping an atom causes it to exhibit extrinsic conductivity.

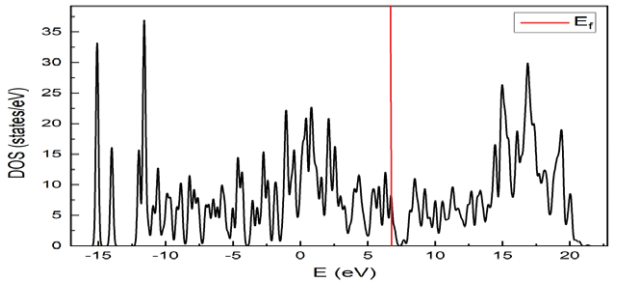

Figure 6) *DOS of In_2C_{34} crystal structure.*

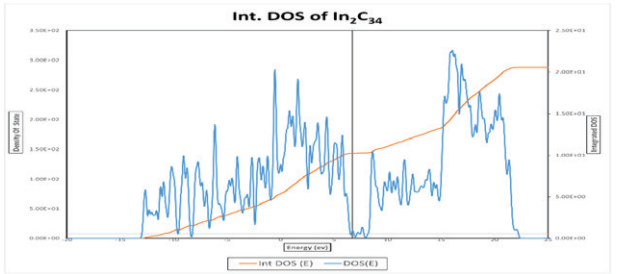

Figure 7) *Integrated DOS of In_2C_{34} crystal structure.*

The structural electronic band configuration of Indium-doped graphene is illustrated in Figure 8. VBM and CBM values generally affect the energy of a material's band gap. By utilizing the distribution of electron energy between the conduction and valence bands, the properties of solid electronic materials can be predicted. The difference in energy between the conduction and valence bands becomes wider by the doping. This results from a charge transfer between Indium and carbon. Valence band maximum lays at 6.8939 eV and the conduction band lays at 6.3488 eV , therefore the energy diffrence berween these two bands is 0.5451 eV.

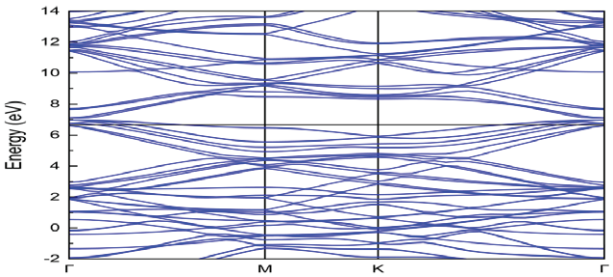

Figure 8) *Band structure of In_2C_{34} crystal structure.*

In_8C_{28} (0.72%)

Now we have modified the calculated values of SCF for 0.72% In doping cells. SCF is converge with a -1388.75646993 Ry energy. As a result, the obtained values are steady and do not change. Convergence has been achieved in 14 iterations.

The In-doped graphene In_8C_{28} crystal structure's entire DOS is depicted in Figure 9. The peak reveals that the Fermi level of graphene doped with indium descends beneath the Dirac point, signifying its classification as a p-type semiconductor. Figure 10 shows the Fermi energy values. In_8C_{28} has an EF of 11.878 eV. Doping an atom causes it to exhibit extrinsic conductivity.

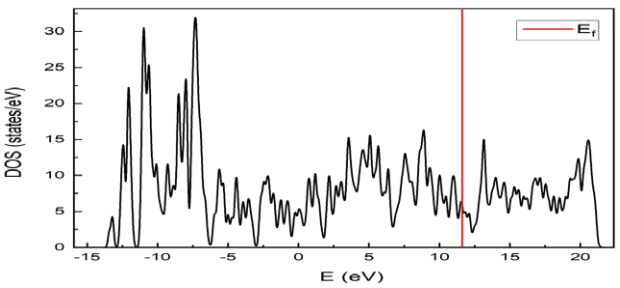

Figure 9) *DOS of In_8C_{28} crystal structure.*

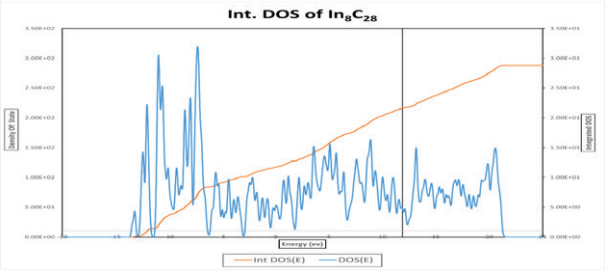

Figure 10) *IDOS of In_8C_{28} crystal structure.*

The structural electronic band configuration of Indium-doped graphene is illustrated in Figure 11. VBM and CBM values generally affect the bandgap energy of a material. The energy dispense of electrons within the valence band and conduction bands can be Used to forecast, the properties of solid electronic materials can be predicted. The difference in energy between the conduction and valence bands becomes wider by the doping. This results from a charge transfer between Indium and Carbon atom. Valence band maximum lays at 11.7986 eV and the conduction band lays at 11.9429 eV , therefore the energy diffrence berween these two bands is 0.1443 eV.

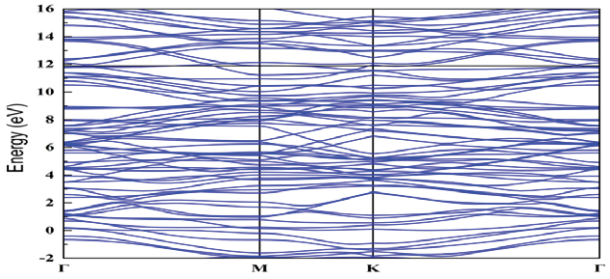

Figure 11) *Band structure of In_8C_{28} crystal structure.*

In our investigation, we have systematically examined the electronic properties of pristine and indium-doped graphene structures, shedding light on their band structure and DOS characteristics. The introduction of indium dopants into graphene induces notable shifts in the Fermi level, underscoring its role as a p-type dopant and thereby altering the material's conductivity behavior. Our analysis of the DOS reveals distinct features indicative of semiconductor behavior, with peaks corresponding to the Fermi level positioned below the Dirac point. Additionally, the examination of band structures elucidates the influence of dopant concentration on the energy dispersions within the valence and conduction bands, providing valuable insights into the bandgap engineering potential of indium-doped graphene.

Antimony-doped graphene

subsequently a concentration of 0.72% (Sb_2C_{34}) and 2.88% (Sb_8C_{28}) of Sb atoms are introduced into pure graphene through doping as shows in Figure 12, illustrates the doping of Sb atoms in graphene. Electronic properties, particularly band structure and DOS, could be estimated using the previously mentioned computational technique.

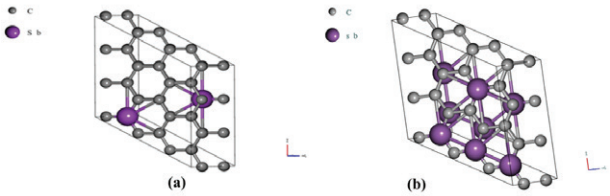

Figure 12) *Crystal structure of antimony doped graphene for (a) Sb_2C_{34} (0.72%) and (b) Sb_8C_{28} (2.88%).*

The presence of the Sb dopant results in an increase in the position of the Fermi level towards the valence band. This effect can be attributed to the fact that the Sb atom has an extra electron compared to a C atom, which allows it to operate as an n-type dopant. such outcome aligns with previous theoretical findings and empirical investigations. The Fermi level undergoes a significant shift beyond the Dirac point, leading to the occurrence of n-type doping. The behaviour of graphene is changed by this phenomenon.

Sb_2C_{34} (0.72%)

Now we have modified the calculated values of self-consistent field SCF for 0.72% Sb doping. SCF is converge with a -421.69875995 Ry energy. As a result, the obtained values are steady and do not change. Convergence has been achieved in 9 iterations.

The Sb-doped graphene Sb_2C_{34} crystal structure's entire DOS is depicted in Figure 13. The peak indicates that the Fermi level of graphene, when doped with antimony, shifts beyond the Dirac point, indicating that it is an n-type semiconductor. Figure 14 shows the Fermi energy values. Sb_2C_{34} has an EF of 7.590 eV. Doping an atom causes it to exhibit extrinsic conductivity, as shown above.

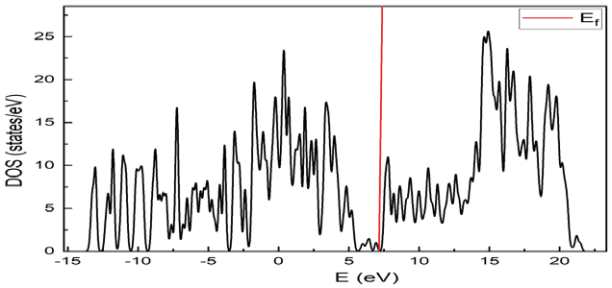

Figure 13) *Density of state of Sb_2C_{34} crystal structure.*

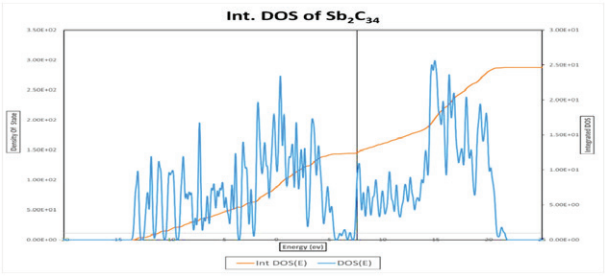

Figure 14) *IDOS of Sb_2C_{34} crystal structure.*

The structural electronic band configuration of Indium-doped graphene is illustrated in Figure 15. VBM and CBM values generally affect the bandgap energy of a material. The energy dispense of electrons within the valence band and conduction bands can be Used to forecast, the properties of solid electronic materials can be predicted. The difference in energy between the conduction and valence bands becomes wider by the doping. This results from a charge transfer between antimony and carbon. Valence band maximum lays at 8.0029 eV and the conduction band lays at 6.4345 eV, therefore the energy diffrence berween these two bands is 1.5684 eV.

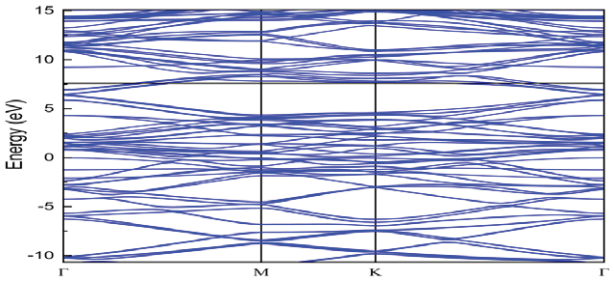

Figure 15) *Band structure of Sb_2C_{34} crystal structure.*

Sb_8C_{28} (0.72%)

Now we have modified the calculated values of self-consistent field SCF for 0.72% Sb doping cells. SCF is converge with a -455.43190615 Ry energy. As a result, the obtained values are steady and do not change. Convergence has been achieved in 13 iterations.

The Sb-doped graphene Sb_8C_{28} crystal structure's entire DOS is depicted in Figure 16. The peak indicates that the Fermi level of graphene, when doped with antimony, shifts beyond the Dirac point, indicating that it is an n-type semiconductor. Figure 17 shows the Fermi energy values. Sb_8C_{28} has an EF of 11.315 eV. Doping an atom causes it to exhibit extrinsic conductivity, as shown above.

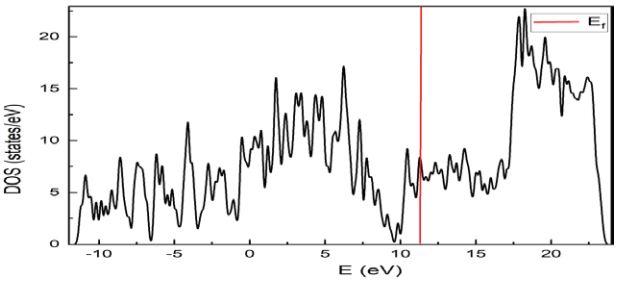

Figure 16) *DOS of Sb_8C_{28} crystal structure.*

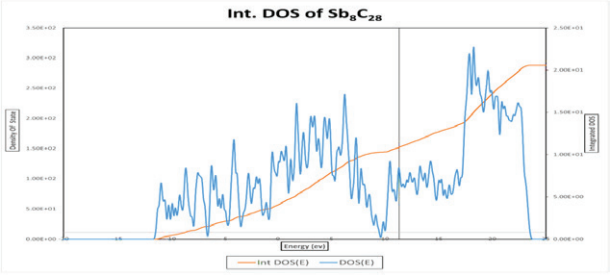

Figure 17) *IDSO of Sb_8C_{28} crystal structure.*

The structural electronic band configuration of Indium-doped graphene is illustrated in Figure 18. VBM and CBM values generally affect the bandgap energy of a material. The energy dispense of electrons within the valence band and conduction bands can be Used to forecast, the properties of solid electronic materials can be predicted. The difference in energy between the conduction and valence bands becomes wider by the doping. This results from a charge transfer between antimony and carbon. Valence band maximum lays at 11.4472 eV and the conduction band lays at 10.8746 eV, therefore the energy diffrence berween these two bands is 0.5726 eV [23-25].

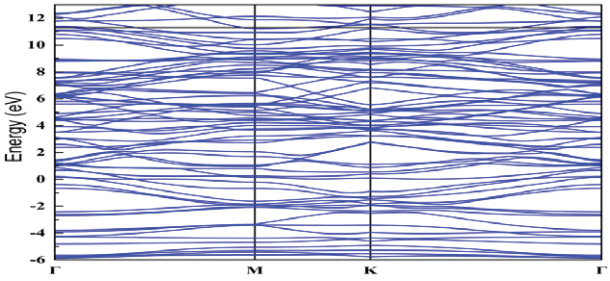

Figure 18) *Band structure of Sb_8C_{28} crystal structure.*

In addition to the computational analysis and characterization provided, it is essential to contextualize these findings within the broader scientific understanding of dopant-induced effects in graphene materials. Recent advances in theoretical frameworks and experimental methodologies have underscored the significance of dopant engineering in tailoring the electronic properties of graphene-based materials. Specifically, the incorporation of antimony dopants introduces additional charge carriers, leading to pronounced shifts in the Fermi level and alterations in the band structure, as observed in our simulations. Moreover, the observed widening of the bandgap due to charge transfer phenomena between antimony and carbon atoms highlights the intricate interplay between dopant species and host material, elucidating potential pathways for engineering desired electronic functionalities. By aligning our results with established theoretical frameworks and empirical observations, our study contributes to advancing the fundamental understanding of dopant-mediated electronic modifications in graphene, paving the way for the rational design and optimization of graphene-based devices for various technological applications. The variation in IDOS reflects changes in carrier concentration, with In-doped graphene exhibiting an increase in hole carriers, while Sb-doped graphene demonstrates a rise in electron carriers. This shift in IDOS correlates with the observed Fermi level shifts and directly influences the material's conductivity and optical properties. In addition to their role in photovoltaic applications, the electronic properties of doped graphene, CdS, TiO_2, and ZnO make them highly relevant for other advanced electronic devices, such as Field-Effect Transistors (FETs) and optoelectronic devices. Field-Effect Transistors (FETs): The ability to tailor the electronic properties of graphene through doping opens up the possibility of fabricating high-performance FETs. By controlling the bandgap and carrier concentration, doped graphene-based FETs could offer faster switching speeds, lower power consumption, and higher stability than conventional silicon-based transistors. Additionally, the integration of materials like ZnO and CdS can further enhance the charge transport and device performance, particularly for flexible electronics. The tunable electronic and optical properties of the doped semiconductors also position them as promising candidates for optoelectronic devices, such as light-emitting diodes (LEDs), photodetectors, and solar cells. For instance, by adjusting the doping concentrations, the bandgap can be engineered to match the required wavelengths for specific applications, while the use of ZnO and TiO_2 as electron transport layers can improve device efficiency by reducing recombination losses. Moreover, the transparent conductive properties of materials like ITO and the enhanced charge separation capabilities of ZnO/CdS composites could lead to novel transparent optoelectronic devices for displays, sensors, and smart windows.

Conclusion

In this study, we explored the electronic properties of In-doped and Sb-doped graphene using DFT calculations, revealing significant bandgap engineering. In-doped graphene exhibits p-type behavior with bandgaps of 0.5451 eV and 0.1443 eV for dopant concentrations of 0.72% and 2.88%, respectively, while Sb-doped graphene shows n-type behavior with bandgaps of 1.5684 eV and 0.5726 eV. These results demonstrate the tunability of graphene's electronic properties, offering potential applications in p-type and n-type devices, including FETs, optoelectronic devices, and solar cells.

However, synthesizing these doped materials presents challenges, particularly in achieving uniform doping and controlling dopant concentrations to avoid clustering and defects. Indium doping in graphene faces limitations due to the low solubility of indium in graphene and the potential for dopant aggregation at higher concentrations. Similarly, Sb-doped graphene may suffer from stability issues and interface defects, which could affect its performance in devices.

To bridge the gap between computational findings and practical applications, several experimental validation steps are necessary. Future work should focus on synthesizing In-doped and Sb-doped graphene using methods like chemical vapor deposition (CVD) or sol-gel techniques, followed by X-ray photoelectron spectroscopy (XPS), Raman spectroscopy, and electrical measurements to confirm dopant distribution and validate the n-type and p-type behavior predicted by DFT. Furthermore, device fabrication using doped graphene can help assess its potential in field-effect transistors, photodetectors, and solar cells, providing experimental evidence for the practical use of these materials.

References

1. Hartree DR. The wave mechanics of an atom with a non-Coulomb central field part I theory and methods. Cam Uni Pres. 1928;24:89-110.
2. Hartree DR. The wave mechanics of an atom with a non-coulomb central field part II some results and discussion. Cam Uni Pres. 1928;24:111-32.
3. Slater JC. The self-consistent field and the structure of atoms. Phys Rev. 1928;32:339.
4. Fock V. Approximate method for solving the quantum mechanical multibody problem. J Phys. 1930;61:126-48.
5. Fock V. Self-consistent field with exchange for sodium. J Phys. 1930;62:795-805.
6. Guerra F, Robotti N. Ettore majorana's forgotten publication on the thomas-fermi model. Phys Persp. 2008;10:56-76.
7. Hohenberg P, Kohn W. Inhomogeneous electron gas. Phys Rev. 1964;136:864-71.
8. Kohn W, Sham LJ. Self-consistent equations including exchange and correlation effects. Phys Rev. 1965;140:1133-8.
9. Goudarzi M, Parhizgar SS, Beheshtian J. Electronic and optical properties of vacancy and B, N, O, and F doped graphene: DFT study. Opto-Electro Rev. 2019;27:130-6.
10. Chen H, Zhao J, Huang J, et al. Computational understanding of the structural and electronic properties of the GeS–graphene contact. Phys Chem Chem Phys. 2019;21:7447-53.
11. Mohamed EA, Mohamed AZ, El-Ela A, et al. ICMMS-2: first-principles investigation of electronic properties of graphene doped with Al and N atoms. Egypt J Chem. 2021;64:1117-23.
12. Tyagi J, Sharma L, Kakkar R. Graphene and doped graphene: a comparative DFT study. Adv Mate Lett. 2019;10:484-90.
13. Rani P, Jindal V. Designing band gap of graphene by B and N dopant atoms. RSC advances. 2013;3:802-12.

14. Rani P, Jindal V. A DFT study of B, N, and BN doped graphene. MRS Online Proce Libr. 2014;1701:7-12.

15. Boadu EO, Abavare EKK, Anderson DE, et al. Poly (9-Vinylcarbazole)/graphene nanoheterostructure interfaces: Ab Initio dynamics studies for photovoltaic and optoelectronic applications. Biointerface Res Appl Chem. 2023;13:1-16.

16. Khan SA, Azam S, Shah FA, et al. Electronic structure and optical properties of the CdO from bulk to nanosheet: DFT approach. Opti Mater. 2015;47:372-8.

17. Karmakar S, Kundu SK, Taki G. The Bandgap study of defects induced graphene structures. 5th International Conference on Electronics, Materials Engineering & Nanotechnology (IEMENTech). Kolkata, India. 2021;pp.01-32.

18. Tahir S, Baluch MA, Mehmood MS. Effect of structural modifications on the electronic characteristics of cadmium oxide: DFT study of oxygen deficit CdO. Uni Wah J Sci Tech. 2023;7:1-10.

19. Perdew JP, Burke K, Ernzerhof M. Generalized gradient approximation made simple. Phys Rev Lett. 1996;77:3865.

20. Andzelm J, King-Smith RD, Fitzgerald G. Geometry optimization of solids using delocalized internal coordinates. Chem Phys Lett. 2001;335:321-6.

21. Grimme S, Antony J, Ehrlich S, et al. A consistent and accurate ab initio parametrization of density functional dispersion correction (DFT-D) for the 94 elements H-Pu. J Chem Phys. 2010;132:154104.

22. Wu M, Cao C, Jiang JZ. Light non-metallic atom (B, N, O and F)-doped graphene: a first-principles study. Nanotechnology. 2010;21:505202.

23. Al-Bagawi AH, Bayoumy AM, Ibrahim MA. Molecular modeling analyses for graphene functionalized with Fe_3O_4 and NiO. Heliyon. 2020;6:e04456.

24. Ezzat H, Menazea AA, Omara W, et al. DFT: B3LYP/LANL2DZ study for the removal of Fe, Ni, Cu, As, Cd and Pb with Chitosan. Biointerface Res Appl Chem. 2020;10:7002-10.

25. Badry R, Radwan SH, Ezzat D, et al. Study of the electronic properties of graphene oxide/(PANi/Teflon). Biointerface Res Appl Chem. 2020;10:6926-35.